Building Simulation 2003

Eighth International IBPSA Conference
Eindhoven, Netherlands
August 11-14, 2003

OCCUPANT RESPONSIVE OPTIMAL CONTROL OF SMART FAÇADE SYSTEMS

Cheol-Soo Park[1], Godfried Augenbroe[1], Nader Sadegh[2], Mate Thitisawat[1], Tahar Messadi[1]
[1]College of Architecture, Georgia Institute of Technology, Atlanta, Georgia, U.S.A.
[2]The George Woodruff School of Mechanical Engineering, Georgia Institute of Technology, Atlanta, Georgia, U.S.A.
Email: cspark@arch.gatech.edu

ABSTRACT

Occupant responsive optimal control is developed for so called smart façade systems. The control optimizes the performance of the system by rotating a motorized louver slat in the cavity and ventilation dampers at the top and bottom of exterior and interior glazing. One prominent feature of the system is the capability of dynamically reacting to the environmental input data through real-time optimization in terms of energy, visual comfort and thermal comfort. Users interaction with the system is Web enabled. Current state variables, weather data and energy flows are posted on a web page and an occupant with given privileges can choose the preferred operation mode or override the devices (louvers, ventilation inlet/outlet).

INTRODUCTION

Windows provide occupants with daylight, direct sunlight, visual contact with the outside and a feeling of openness. However, glazing may cause a number of problems: excessive undesired heat gain (loss) due to its high U-value. An over-lit window surface can also cause glare, which is a major complaint by occupants. Furthermore, cold or hot window surfaces induce asymmetric thermal radiation which can result in thermal discomfort.

To reduce the potential problems of window systems, double skin façades and airflow window systems have been introduced in the 1970s. They typically contain interstitial louvers and ventilation openings that enforce different airflow regimes through the glass enclosed cavity in summer and winter.

The current problem with double skin façades and airflow windows is that their operation requires adequate dynamic operation to reach their expected performance. Many studies have recognized that only an optimal control of the louver slat angle and airflow regime enables these systems to truly act as active energy savers and indoor environmental controllers. However, an adequate control strategy for this dynamic optimization problem has thus far not been developed (Rippati [1984], Mueller [1984], Wright [1986], Barakat [1987], Hayashi [1989], Cho [1995], Haddad [1998], van Paassen [2000], Saelens [2002]). One recently reported control strategy that was applied to the Helicon building, a £28 million project in London is quite straightforward (CIBSE, 1996). The fundamental principle of the applied control is a rule-based approach where the blinds are lowered to the horizontal position when the solar radiation incident on the façade reaches a threshold (150W/m2).

Lack of such a dynamic control is because of the following challenges:

First, an adequate control needs an underlying mathematical model to predict the response of a system. But, the nature of the dynamics of these systems involves complex irregular 3D geometry where turbulent air flows and each solid and non-solid component is linked to other components by radiative and convective heat exchange, and thus it is not easy to accurately predict the response of the system in computations.

Second, it is difficult to apply modern analytical optimal control theory such as Pontryagin's Minimum Principle because of high nonlinearity of the physical mathematical representation of the system, complicated by the change of the airflow regime and thus of the mathematical representation. In addition, the occupant's intervention further complicates the application of the optimal control theory.

Third, the systems are expected to reflect the multifaceted user preference such as energy conservation, visual comfort and thermal comfort. The determination of optimal control actions synthesizing these three major system utilities is a complex tradeoff influenced by heating, cooling, and lighting loads, exterior and interior glazing temperature, outdoor and indoor air temperature, solar radiation, sky condition, personal preference, etc. The above-mentioned set of state variables and parameters woven with the multifaceted quantitative and qualitative cost elements explain the difficulty to determine optimal control actions.

To overcome these difficulties, so-called smart façade systems have been introduced as shown in Figure 1. They have a smart controller that operates

a motorized Venetian louver system and ventilation dampers, in order to combine the benefits of large windows with low energy demands for heating and cooling, while keeping visual well-being and thermal comfort at an optimal level. Smart façade systems are controlled by an optimization routine with an embedded simulation model. The control system is occupant responsive via Web enabled access.

Figure 1. Smart Façade Demo Unit (SFDU) installed in the College of Architecure building, Georgia Institute of Technology, U.S.A.

MATHEMATICAL MODEL

In order to describe the dynamics of smart façade systems, the following heat and mass transfer phenomena governing heat transport processes are studied: 1) Direct, diffuse and reflected solar radiation. 2) Long wave radiation between surfaces. 3) Convective heat transfer along exterior glazing, interior glazing, and louver slats. 4) Air movement through inlet/outlet dampers and the cavity.

As briefly addressed in the introduction, the complexity of the problem should be recognized. The smart façade system involves transient convective, conductive and radiative heat transfer and turbulent air flows in irregular 3D geometry with boundary conditions constituted by outside temperature and solar radiation, etc. In addition, while actually simulating the dynamics of the system, adequate optimal control actions must be determined in real-time, effects of which are dynamically coupled with the dynamics of the system of a highly nonlinear nature.

Thus, in order to describe the dynamics of the smart façade system solvable with reasonable efforts, a lumped physical model had to be developed as follows.

By assuming the heat transfer in the lateral direction to be negligible, the thermal behavior of smart façade systems can be reduced to a 2D model as illustrated in Figure 2. Next, we lump the exterior glazing temperature, the interior glazing temperature, the louver temperature, and the cavity air temperature in the vertical direction. Although this cannot render the explicit vertical temperature gradients due to the convective flow effects in the cavity, this vertical lumping of the glazing temperatures is assumed to have little effect on representing the overall thermal characteristics of smart façade systems and on determining optimal control actions. This has, of course, to be substantiated by experiments.

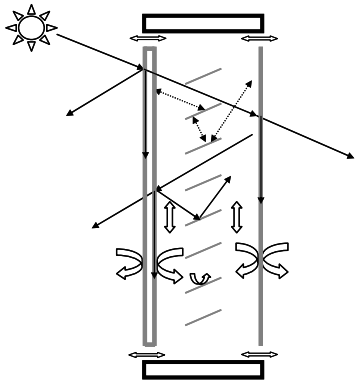

Figure 2. Simplified system in 2D

In mathematically formulating the direct, diffuse and reflected solar radiation and long wave radiation between surfaces, we used the theoretical model suggested by Rheault et al (1989) without much modification. Based on the assumption of a fictitious cavity bounded by adjacent louver slats and interior and exterior glazing, the direct and diffuse solar radiation, and its reflection are calculated.

In the modeling of the convective heat transfer, the six unknown convective heat transfer coefficients ($h_{out}, h_{ca,1}, h_{ca,2}, h_{ca,3}, h_{ca,4}, h_{in}$) (Figure 3) should be estimated because the literature values of those coefficients presented in (ASHRAE 1997), (Clarke 2001), (Incropera 1996) are empirically driven for general cases and thus, can significantly vary according to the system configuration, location, surroundings, the nature of surface, meteorological environment, etc. Especially, the convective heat transports in the cavity occur with rotating curved louver slats in the various airflow regimes (upward or downward airflow either in the closed cavity or the open cavity). Unfortunately, there is very limited data available on these behaviors. Thus, these coefficients are estimated with parameter estimation technique, based on the extensive data points obtained from experiments. This will be discussed in the following section.

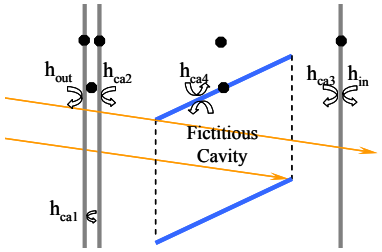

Figure 3. Unknown convective heat ransfer coefficients (●: state variables)

The remainder of this section will therefore only concentrate on the modeling of air movement through the inlet/outlet dampers.

Firstly, ten possible airflow regimes have been selected as illustrated in Figure 4. In Mode #1~2 the upper and lower dampers are open (*inside circulation*) and Mode #3~4 are reversed (*outside circulation*). For Mode #1~2, air circulating between the room and the cavity is driven by thermal buoyancy while in Mode #3~4, air circulation is driven by thermal buoyancy and wind pressure. Modes #5~8 allow a *diagonal airflow* either from inside to outside or vice versa. Mode #9 and #10 respectively represent the cases where the four dampers are open/closed.

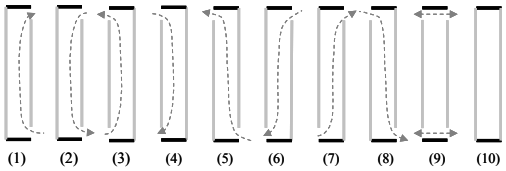

Figure 4 Ten airflow regimes (louver slats not drawn for clarity)

The modeling of the airflow in Mode #1~2 is discussed in Park et al (2002). It is based on a conventional one-dimensional formulation utilizing momentum and energy conservation. By combining the momemtum equation and the total flow resistance parameter, the mean air velocity in the cavity, u_m, is solved algebraically as:

$$u_m = u_b = \sqrt{2}\frac{h}{d}\sqrt{\frac{gL}{k}\left(\frac{T_{ca}-T_\infty}{T_\infty}\right)} \qquad (1)$$

where h is a open height of the ventilation damper, d is the depth of the cavity, g is the gravity acceleration, L is the height of the cavity, k is the form loss factor, T_∞ is the indoor air temperature and T_{ca} is the cavity air temperature.

In modeling the outside circulation loop (Mode #3-4), the pressure difference between upper and lower openings, as a result of wind effect, must also be accounted for. As wind forms a boundary layer over the ground surface, wind velocity and hence wind pressure at upper opening are expected to be higher than those at the lower opening. Thus, for wind flowing perpendicular to the façade, it is reasonable to expect downward airflow within the cavity. Consequently, the influence of wind on vertical pressure gradient is expected to be larger at higher distances from the ground level, resulting in a much larger pressure difference on the facade of a high-rise building (Saelens 2002).

The overall wind pressure, or velocity pressure, is given by the Bernoulli equation:

$$p_w = C_p \rho \frac{V^2}{2} \qquad (2)$$

where C_p is the discharge coefficient, ρ is air density and V is wind velocity. Considering the difficulty in characterizing the airflow rate through the dampers, the power law equation, is applied to approximate the relationship between the volumetric air flow rate (Q) and pressure difference (Δp):

$$Q = c(\Delta p)^n \qquad (3)$$

where c is the flow coefficient and n is the flow exponent. Integrating (5) and (6) yields:

$$u_w = \frac{c}{A_c}\left(C_p \rho \frac{V^2}{2}\right)^n \qquad (4)$$

where A_c is the cross-sectional area of the cavity.

The next step is to combine the air flow rate caused by buoyancy (Q_b) and by wind pressure (Q_w). A simpler model (Sherman 1992) suggests the following equation:

$$Q = \sqrt{Q_b^2 + Q_w^2} \qquad (5)$$

Finally, the air velocity caused by buoyancy and wind can be derived by combining Eq. (1) and (5).

$$\begin{aligned} &if\ C_p \geq 0 \\ &\quad \begin{cases} if & u_b \geq u_w : u_m = \sqrt{u_b^2 - u_w^2} \\ elseif & u_b < u_w : u_m = -\sqrt{u_w^2 - u_b^2} \end{cases} \\ &elseif\ C_p < 0 : \qquad u_m = \sqrt{u_b^2 + u_w^2} \end{aligned} \qquad (6)$$

Eq. (6) indicates that when C_p>0, the wind blows toward the façade surface and reverses the air flow in case that the wind-driven downward airflow overweighs the buoyancy-driven upward airflow ($u_b < u_w$). When C_p<0, the pressure becomes negative and the wind increases upward air flow.

The modeling of the diagonal airflow (Mode #5,6,7,8) includes one more driving force besides buoyancy (P_b) and wind (P_w): static pressure difference (P_s) caused by the (de)pressurization of an interior space. The static pressure difference can be very significant because modern office buildings are air-tight and usually pressurized in order to limit untreated outdoor air leaks into the interior (infiltration) as a means of minimizing HVAC loads and related operating costs (ASHRAE 1997).

The total pressure difference (ΔP) caused by the temperature difference, wind and stack pressure is:

$$\Delta P = P_b + P_w + P_s \qquad (7)$$

By using the nodal network method (Hensen 1991), the buoyancy pressure difference(P_b) is calculated.

Based on the Δp in Eq. (7), the volumetric air flow (Q) can be approximated by the power law equation and the mean air velocity becomes:

$$Q = c(\Delta p)^n = c(P_w + P_b + P_s)^n \quad (8)$$

$$u_m = \frac{Q}{A_c} = \frac{c}{A_c}(P_w + P_b + P_s)^n \quad (9)$$

Note that Mode #9 in Figure 4 is considered inappropriate to be used in the lumped model approach because it requires more complex modeling and information.

Based on what has been discussed above, the mathematical model is developed for the following six state variables, comprising the temperatures of: each glazing of the exterior double pane, the cavity air within the double pane, the larger cavity air, the louver slats, and the interior glazing (Figure 3). The mathematical model is expressed in the continuous state space form as shown in Eq. (10).

$$\dot{x} = A(u,t)x + b(u,t) \quad (10)$$

where x is the state vector, A is the state matrix, b is the load vector, and u represents the control variables. It should be noted that the room or the building model is not part of the state space model, which means that the smart double-skin façade system is treated as a 'local' system and hence a local control problem, i.e., based purely on local state information. The benefit of isolating the smart double-skin façade system is that the resulting façade component with its embedded optimal control can become a part of any building model. If the smart double-skin façade system needs to be incorporated into a room or a building model, a set of differential equations for other states such as floor, ceiling, and walls can be added to Eq. (10) for a simultaneous solution.

Note that the dependency of A on u results in a system that is nonlinear in u. This is prohibitive to a numerical state space solution. By converting the continuous (in time) state space (10) to a discrete (in time) state space, Eq. (11), this nonlinearity disappears because $u_k = constant\ for\ t_k \le t \le t_{k+1}$.

$$x((k+1)T) = G(T)x(kT) + H(T) \quad (11)$$

where $G(T) = e^{AT}$, $H(T) = A^{-1}(e^{AT} - I)b$, and T is the sampling time.

PARAMETER ESTIMATION

As discussed in the previous section, the lumped ('minimalistic') model includes unknown parameters such as the convective heat transfer coefficients (Figure 3), the form loss factor (k) in Eq. (1), the flow coefficient and exponent (c, n) in Eq. (4) and (9).

The parameter estimation is the process of calculating the unknown parameters for a system which minimize the deviation between model output and measurement output. This can be formulated into minimizing an objective function S over the measurement period as follows:

$$\min\ S = \sum_{k=1}^{n} [Y_k - \psi_k(\xi)]^T [Y_k - \psi_k(\xi)] \quad (12)$$
$$s.t.:\ lb \le \xi \le ub$$

where Y_k is the observation vector at time k, ψ_k is the predicted vector of observations, n is the number of observations, ξ is the vector of unknown parameters and lb and ub are the vectors of lower and upper bounds of the parameters.

In this study, a function called 'LSQNONLIN' in the MATLAB optimization toolbox is employed to solve for Eq. (12) because it is specially designed to solve this kind of nonlinear least squares problems subject to inequality constraints, and to expeditiously generate a reliable estimate of the solution.

The Figure 5 shows the validation result, comparing the calibrated model and the measurement with another period of time (03/24/2003-03/29/2003). The average temperature difference between the simulation and the measurement is 1.51˚C.

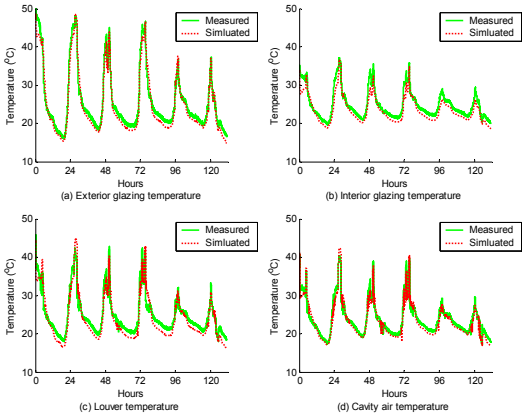

Figure 5. Validation of the simluation model

OCCUPANT RESPONSIVE OPTIMAL CONTROL

The overall performance of smart façade systems can be categorized into three elements, which account for three major system utilities: energy use, visual comfort and thermal comfort. The cost elements in energy utility include convective and radiave heat transfer loss(gain), solar radiation transmission, and beneficial use of the cavity airflow regime. The cost elements in visual comfort include average daylight illuminance, uniformity, average luminance of the inteiror window surface, outward visibility through the slats, and daylghting autonomy. The thermal

comfort is expressed in Predicted Mean Vote (PMV). Each utility consisting its sub element can be formulated in the cost function (J) as follows.

$$J = \int_{t1}^{t2} \begin{bmatrix} r_1\left(h_{in} A\left|x_2 - x_{room}\right| + Q_{solar,trans} + Q_{air}\right) \\ +r_2 pf_1\left(E_{avg}\right) + r_3 pf_2\left(U\right) + r_4\ pf_3\left(L_{avg}\right) \\ +r_5 pf_4\left(\varphi\right) + r_6 pf_5\left(DA\right)^2 + r_7\left(PMV\right)^2 \end{bmatrix} dt \quad (13)$$

where r_i are the relative weighting factors, A is the area of interior glazing, x_2 is the interior glazing temperature, x_{room} is the room air temperature, $Q_{solar,\,trans}$ is the sum of transmitted direct and diffuse solar radiation, Q_{air} is the cooling and heating load reduction by beneficial airflow regime from the cavity to the room space or outside, pf_i are the square penalty functions, E_{avg} is the average daylight interior illuminance on the work plane, U is the uniformity, L_{avg} is the average window luminance, φ is the louver slat angle, and DA is the daylighting autonomy. The prediction of inteiror daylight luminous distribution, the selection of the visual performance criteria, the square penalty functions are discussed in detail in (Park et al 2003).

The optimal control attempts to find the control actions which minimize the cost function (J) over a certain period of time as shown in Eq. (14).

$$\begin{aligned} &\min J\left(\varphi,\ AFR,\ OR\right) \\ &s.t.:\ -90° \le \varphi \le 90° \\ &\quad AFR = 1, 2, 3, 4, 5, 6, 7, 8, 9, 10 \\ &\quad 0 \le OR \le 100(\%) \end{aligned} \quad (14)$$

where AFR is the airflow regime mode (Figure 4), and OR is the opening ratio of ventilation dampers. Due to the nonlinearity of the dynamics of the system and additional constraints on the control variables, it is difficult to find the optimal control actions (slat angle, opening ratio, airflow regime) analytically. Additionally, since the airflow regime is expressed as an integer from 1 to 10, the current problem consisting of continuous and discrete control variables leads to a combinatorial problem (Winston, 1994), which is unrealistic to solve.

Thus, the discrete airflow regime (AFR) is translated as a continuous variable (AFR*). When $n \le AFR^* \le n+1$, the AFR is defined as n and the opening ratio (OR) is determined as shown in Figure 6.

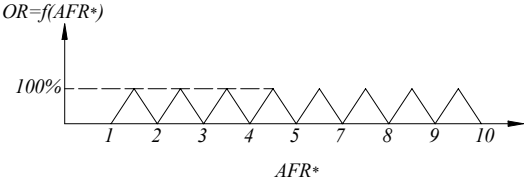

Figure 6. Converting discrete variable (AFR) to continuous variable (AFR)*

Then, to deal with the problem numerically, the function 'FMINCON', one of the MATLAB optimization routines was employed. The function 'FMINCON' finds a minimum of a constrained nonlinear function of several variables starting at an initial estimate. Inside the function 'FMINCON', the discrete state space and the cost function are described with the sampling time (T) of 15 minute, which is small enough for these slowly time-varying systems. And, the time horizon is set equal to 3hours.

REAL APPICATION OF OCCUPANT RESPONSIVE CONTROL

The architecture of the occupant responsive optimal control for the demo unit is shown in Figure 7. The local server logs input data from the demo unit and the weather station. Based on the logged data, the MATLAB optimization routine embedded in the local server finds the optimal control actions, the actuation commands are transmitted from the local server to the actuators. The smart controller programmed in a local server actuates motors to rotate the louver slat angle and to open/close the ventilation inlet/outlet dampers. The local server posts a live update of the current status (states, weather, WEBCAM image) and the potential energy savings (Figure 8, 9) on the Web.

Figure 9 shows the Web interface for an occupant with given privileges to choose the preferred mode (energy saving mode, visual comfort mode, thermal comfort mode, autonomous mode [three system utilities concerned based on the user' s weighting system]) or override the devices from anywhere in a building through a standard browser. This web interface is developed with Microsoft .NET ASP web application and the LabVIEW 6.1.

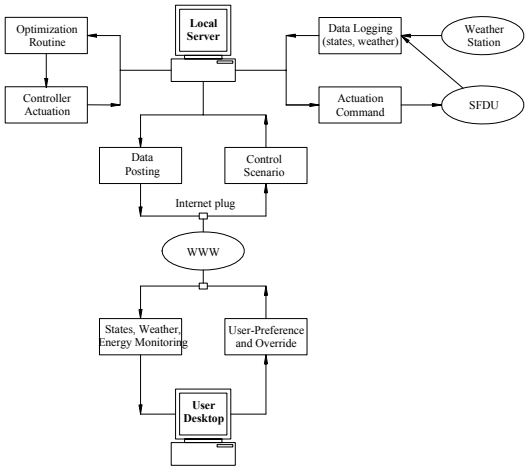

Figure 7 Architecture of the occupant responsive optimal control of rhe demo unit

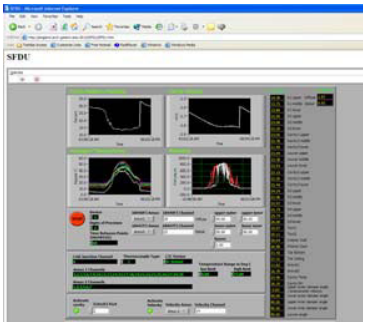

Figure 8 Real time data posting on the Web

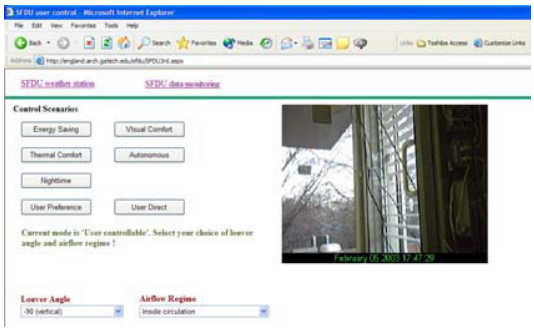

Figure 9 Web allowing occupant's selection of control modes (http://england.arch.gatech.edu/sfdu/)

OPTIMAL CONTROL SIMULATIONS

Optimal control simulations were accomplished for a winter, summer and fall day under clear, intermediate and overcast sky with 4 different control scenarios (energy, visual, thermal, autonomous). For want of space, only the simulation under a clear winter day in energy saving mode is discussed below.

Figure 10(a) shows the calculation of the state variables. Figure 10(b)~(c) shows that the optimal louver slat angle keeps track of the solar altitude so that it can absorb direct solar radiation during daytime. At nighttime, the louver slat angle stays at 90˚ such that it can reduce heat loss by longwave radiation between the interior glazing and the colder exterior glazing. It is also interesting that a louver angle of 90˚ occurs around sunrise and sunset time. It can be inferred that around sunrise and sunset time the heat loss by longwave radiation between the interior and the colder exterior glazing is more than the heat gain from absorbing weak solar radiation.

As shown in Figure 10(d), the airflow regime during daytime is Mode #1 (Figure 4). In that mode the hot cavity air circulates into a room space for the reduction of heating load. At nighttime, Mode #5 airflow regime occurs so that the exhausted air warms the cold cavity. Mode #5, is useful and can be considered 'a local heat exchanger' as it uses exhaust air to heat up the façade system thus reducing transmission losses. The ventilation dampers are open all day in either Mode #1 or #5 and the opening ratio of the dampers are almost 100% as shown in Figure 10(e), which means maximizing the beneficial use of airflow. The dominant driving force for diagonal airflow (Mode #5) is the static pressure difference(P_s). The estimated static pressure difference (due to the pressurization of the building due to air supply through the HVAC system) from the laborious experiment is 4.2 Pa. Thus, the airflow velocity profile in Mode #5 (Figure 10(f)) is flat with the stationary P_s .

Figure 10(g)-(j) shows the daylighting performance in energy saving mode. The average daylighting illuminance, the luminance and the uniformity are far beyond the threshold values and this will cause visual discomfort.

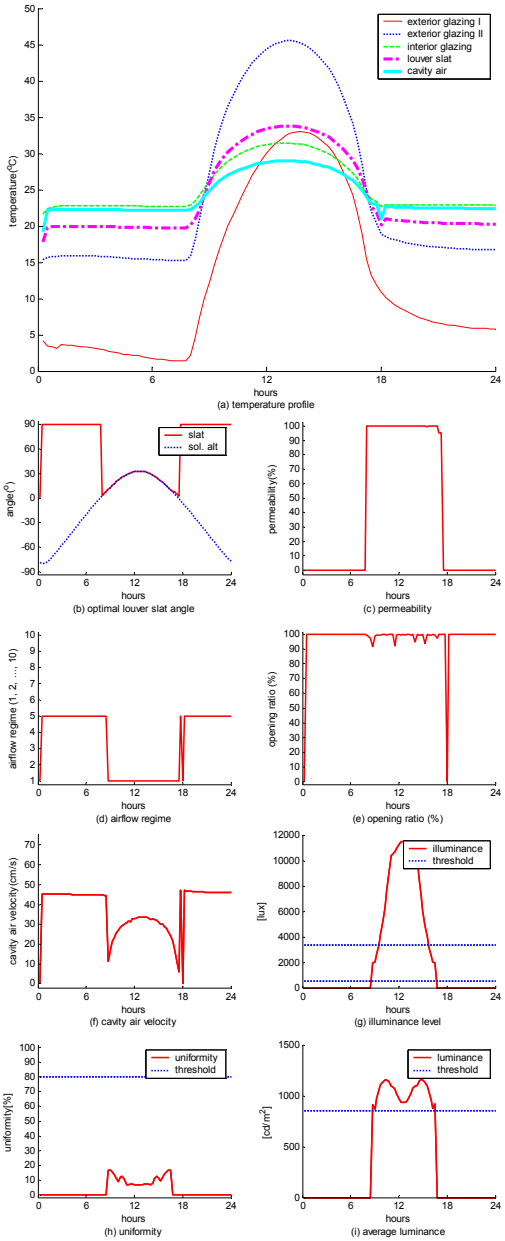

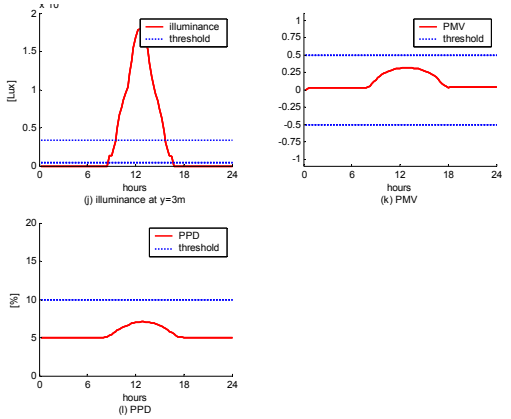

Figure 10 Optimal control simulation under a clear winter day

It is interesting that the maximum interior glazing temperature is very low (31.4˚C) compared to general window systems because the cavity air circulates during all hours of the daytime. Conseqently, the values of PMV and PPD are in the comfortable range. The maximum PMV and PPD is 0.3164 and 7.08%, respectively (Figure 10(k), (j)).

COMPARATIVE STUDY

The performance of smart façade system (System I) is compared with a manually-controlled façade system (System II) having an identical specification as System I except that optimal control is replaced by manual actions and a conventional window system (System III) consisting of 6mm clear +6mm low-e separated by 12.7mm air space and indoor shading by Venetian blinds. The comparative study is conducted for the climate of Atlanta, GA (33.65N, 84.42W) in summer and winter day under CIE sky condition (clear, intermediate, overcast).

For better quantitative representation of the system's performance and easy comparison, a number of performance indicators are introduced as shown in Table 1.

Table 1 Performance Indicators (PIs)

Utilities	Performance Indicators (PIs)
Energy	Energy efficiency coefficient (η)
Visual comfort	*8 performance indicators are presented in Park et al (2003)*
Thermal comfort	Average PPD
	% of hours in comfort range (<10%)

The system energy efficiency coefficient (η) is the ratio of the amount contributed by the system to the cooling (heating) load reduction of the room space to the total solar radiation received by the exterior glazing ($Q_{solar,ext}$). For example, in heating mode, the reduction of heating load in the room is the sum of transmitted solar radiation, the heat transfer by beneficial airflow from the cavity to the room, and the convective heat transfer occurring at the interior glazing surface (Q_{conv}). In cooling mode, the reduction of cooling load in the room can be obtained by summing up the amount of solar radiation blocked by the system compared to the total solar radiation received by the exterior glazing. The system energy efficiency coefficient in heating mode can be formulated:

$$\eta = \left(Q_{solar,trans} + Q_{air} + Q_{conv}\right) / Q_{solar,ext} \qquad (15)$$

In a similar way, the system energy efficiency coefficient in cooling mode can be calculated.

Table 2 shows the energy performance comparison of the System I to System II and III for winter and summer day (Dec. 22nd, Jun. 22nd) under clear sky condition.

Table 2. Energy performance comparison (η)

	Sys. I	Sys. II	Sys. III
Heating mode(winter)	34.0	8.7	30.1
Cooling mode(summer)	99.0	94.7	84.5

In heating mode, System III performs better than System II because System III has one less glazing and no blinds in the cavity, resulting in easy penetration of solar radiation into a room space. In contrary, System III is worst in cooling mode. System I surpasses the other two systems in both seasons.

Table 3 shows comparison of annual primary energy savings ($) calculated by extrapolation.

Table 3 Energy savings in $/m2/yr

	Sys. I – Sys. II	Sys. I – Sys. III
Heating mode	73.0	11.7
Cooling mode	6.7	22.5

* Assumption:
- *Energy price: $0.075/KWh (PNNL 2002)*
- *Work days per year: 5days*52weeks*
- *Efficiency of power generation: 39% (NEN 2916)*

Note that the energy saving effect in Table 3 is for the case of south-facing systems. Considering an amount of the solar radiation normal to the surface of east or west facing systems, the saving effect of System I will increase.

CONCLUSION AND FUTURE WORK

It has been shown that lumped models for double façade components can be easily constructed and augmented by parameter estimation. These calibrated parameters compensate for errors introduced by the space averaging and other model simplifications. The resulting model was validated through laborious

experiments during which the unit was subjected to different control actions, ventilation regimes, and stark variations in weather conditions. The model proved surprisingly accurate in the prediction of the most relevant state variables and very reliable for energy, comfort and lighting design studies.

Based on the prediction of the lumped 'calibrated' model, the MATLAB optimization routine can effectively determine the control actions in on-line real-time. Through the performance comparison of smart façade system to a manually-controlled façade system and a conventional window system, it can be concluded that smart façade systems are more advantageous in terms of energy, visual comfort and thermal comfort.

Following the successful development of optimal control and its implementation, future study may include: 1) Development of a parameterized software module of façade elements in whole building simulation packages, e.g. for use in Energy-Plus. 2) Feasibility and applicability study of this type of facade technologies, looking at physical, economical, durability, controllability and systems integration aspects. 3) Application of the on-line real-time optimization framework to a variety of building systems (mechanical systems, lighting control systems) either as a stand-alone or as a whole-HVAC integrated building automation system.

REFERENCES

ASHRAE 1997. *ASHRAE Handbook Fundamentals*, ASHRAE.

Barakat, S.A. 1987. Thermal Performance of a Supply-Air Window, *Proc. of the 12th Annual Passive Solar Conference* 12: pp.152~158

Cho, S.H., Shin, K.S., and Zaheer-Uddin, M. 1995, The Effect of Slat Angle of Windows with Venetian Blinds on Heating and Cooling Loads of Buildings in South Korea, *Energy*, Vol.20, No.12, pp.1225~1236

CIBSE. 1996. City Slicker, *CIBSE Journal*, Vol.18, No.9, pp.20~24

Clarke, J.A. 2001. *Energy Simulation in Building Design*, Butterworth-Heinemann

Dutch Standard NEN 2916. 1998. *Energy Performance of Non-residential Buildings: Determination method*

Haddad, K.H., and Elmahdy, A.H. 1998. Comparison of the Monthly Thermal Performance of a Conventional Window and a Supply-Air Window, *ASHRAE Transactions*, Vol.104, Part 1B, pp.1261~1270

Hayashi, T., Katayama, T., Sugai, T. and Watanabe, T. 1989. Time-Variable Numerical Model of Heat Transfer around Solar Shading Device on Windows, *Proc. of the ASHRAE/DOE Conference on Thermal Performance of the Exterior Envelopes of Buildings IV*, pp.405~413.

Hensen, J.L.M. 1991. *On the thermal interaction of building structure and heating and ventilation system*, Ph.D. thesis, University of Eindhoven

Incropera, F.P. and DeWitt, D.P. 1996. *Introduction to heat transfer*, John Wiley & Sons, 3rd Ed.

Mueller, H.F.O. 1984. Exhaust air ventilated windows in office buildings, *ASHRAE Transactions*, pp.932~947

Pacific Northwest National Laboratory (PNNL). 2002. *Building Energy Data Book*, PNNL

Park, C.S., Augenbroe, G.L.M., and Sadegh, N. 2002. Development of Optimal Predictive Control of Smart Façade Systems, *Proc. of 2nd International Postgraduate Research Conference in the Built and Human Environment*, April 11~12, Salford, U.K.

Park, C.S. Augenbroe, G.L.M., and Messadi, T. 2003. Daylighting optimization by smart façade systems, *Proc. of IBPSA Conference*, Eindhoven, Netherlands

Rheault, S. and Bilgen, E. 1989. Heat Transfer Analysis in an Automated Venetian Blind Window System, *Journal of Solar Energy Engineering*, Vol.111, No.1, pp.89~95

Ripatti, H. 1984. Airflow window system - Making fenestration the solution rather than the problem in energy use, *ASHRAE Transactions*, Vol.90, Part 1B, pp.917~931

Saelens, D. 2002. *Energy Performance Assessment of Single Storey Multiple-Skin Façades,* Ph.D. Dissertation, Katholieke Universiteit Leuven

Sherman. 1992. Superposition in Infiltration Modeling, *Indoor Air* 2:101-14

Winston, W.L. 1994. *Operations Research,* Duxbury Press

Wright, J.L. 1986. Effective U-values and shading coefficients of preheat/supply-air glazing systems, *Proc. Solar Energy Society of Canada*

van Paassen, D. and van der Voorden, M. 2000. Development of Simplified Tools for Evaluation Energy Performance of Double Façade, Proceedings of International Building Physics Conference, pp.347~355